Check for updates

Dependence of electrochemical properties of spinel LiMn$_2$O$_4$ on Li$_2$CO$_3$ with micro-flaky, micro-flower and nanorod morphologies†

Lang Li, Jinsong Sui, Rui Huang, Wei Xiang and Wei Qin [ID] *

Herein, the dependence of spinel LiMn$_2$O$_4$ on Li$_2$CO$_3$ with micro-flaky, micro-flower and nanorod morphologies is investigated. The results show that the as-synthesized LiMn$_2$O$_4$ with micron sized Li$_2$CO$_3$ as raw materials have a much higher discharge capacity than that of the one prepared with nano sized Li$_2$CO$_3$. It delivers an initial charge capacity of 110.1, 105.2 and 104.9 mA h g^{-1} followed by a discharge capacity of 109.1, 103.9 and 104.2 mA h g^{-1} with the micro-flower, nanorod and micro-flaky Li$_2$CO$_3$ morphologies, respectively, at room temperature (about 99% of the charge capacity is discharged). The smaller specific surface area is found in the spinel LiMn$_2$O$_4$ with micron sized Li$_2$CO$_3$, resulting in a better stable electrochemical performance in LiMn$_2$O$_4$ with micro-flower and micro-flaky Li$_2$CO$_3$. Their capacities are maintained at 99.2 mA h g^{-1} and 94.2 mA h g^{-1} after 100 cycles at 1C rate. The capacity retention was more than 90% at the 100th cycle with the micron-sized Li$_2$CO$_3$. Moreover, the as-synthesized spinel LiMn$_2$O$_4$ with micro-flower Li$_2$CO$_3$ retained more than 95% of its initial discharge capacity (92 mA h g^{-1}) after 200 cycles at 2C rate. The cubic spinel structure was detected after 200 cycles of LiMn$_2$O$_4$ at 2C rate.

Introduction

Rechargeable batteries are becoming increasingly important recently, particularly in consumer electronic devices such as cellular telephone, notebook computers, compact camcorders, and electronic vehicles.[1–4] Spinel LiMn$_2$O$_4$ is regarded as one of the most promising cathode materials for lithium ion batteries[5] by virtue of its obvious advantages such as abundant and cheap resources, environmental friendliness, safe handling and low toxicity.[6,7] However, the disadvantages of structural instability, poor cycle efficiency and low energy density have held back its application for large scale production. In general, as for the battery application, LiMn$_2$O$_4$ powder should possess a single-phase, homogeneity, uniform particle morphology with a submicron size distribution, and a large surface area in order to achieve better electrode properties. The factors such as crystallinity, crystal structure, the deviation from theoretical stoichiometry of elemental composition as well as the grain size and its distribution play important and eventually, decisive roles in the electrochemical performance of spinel LiMn$_2$O$_4$. The compound was typically obtained by reaction of a mixture of a lithium salt and manganese oxides subjected to high temperature in air for several hours.

Department of Chemical Engineering, State Key Laboratory of Chemical Engineering, Tsinghua University, Beijing 100084, China

† Electronic supplementary information (ESI) available. See DOI: 10.1039/c7ra07088h

However, the preparation of spinel LiMn$_2$O$_4$ involves the solid-state reactions starting from the raw materials, such as manganese oxides, nitrate or carbonate with lithium hydroxide, nitrate or carbonate at elevated temperatures as high as 700–900 °C. The final products usually contain larger irregular particles, with a broad size distribution, as well as impurity phases. Furthermore, this method could not provide a good control on the crystalline growth, compositional homogeneity, morphology, and microstructure. To overcome these problems, the purity and particle size distribution of Li$_2$CO$_3$ as the cathode material were optimized. Moreover, the reaction process of Li$_2$CO$_3$ and MnO$_2$ was studied using thermogravimetry (TG), derivative thermogravimetry (DTG) and differential scanning calorimetry (DSC). A uniform cubic nanostructured spinel LiMn$_2$O$_4$ fused together was obtained. The most suitable calcination temperature was programmed using an oven.

Recently, many studies have been conducted to improve the performance of rechargeable lithium ion battery by using cationic doping[8,9] and the nanostructured electrode[10,11] that have shown to enhance power performance due to the large surface-to-volume ratio that allows for a large electrode–electrolyte contact area. Nanocrystal,[12] nanoporous,[13] nanorod,[14] nanotube,[15–17] nanowire[18,19] and nanotube active materials are particularly attractive. The disadvantage of nanosized materials is that they cannot be packed as dense as the micron-sized materials on the current collector, since the electrodes made of nanosized materials exhibit a high porosity, thus resulting in a decrease in the cell capacity. Therefore, the best way to

improve both the rate capacity and the electrode density would be to use the micron-sized particles that consist of aggregated nanoparticles.[20] Most of the nanostructured electrode materials are synthesized by low-temperature treatment processes such as soft chemical,[21] sol–gel,[22,23] and hydrothermal methods.[24] However, little attention has been paid to the effect of the purity and the morphology of the cathode material Li_2CO_3.[25] In this paper, the cubic uniform nanostructured spinel $LiMn_2O_4$ fused together was synthesized by the solid state reaction with Li_2CO_3 in micro-flaky, micro-flower and nanorod forms. Moreover, the electrochemical characteristics of the as-synthesized spinel $LiMn_2O_4$ were compared with each other to determine the most suitable morphology and size of the raw materials.

Here, a novel strategic synthesis process of a battery grade lithium carbonate was carried out in a homogeneous-like organic phase.[26] Three types of crystal morphology were prepared: micro-flower, micro-flaky, and nanorod. The nanostructured spinel $LiMn_2O_4$ was then synthesized by the solid-state reaction with MnO_2 (EMD) with a calcination program at high temperature. The electrochemical performances of the prepared spinel $LiMn_2O_4$ were discussed. The result showed that the nanostructured spinel $LiMn_2O_4$ prepared with the micron sized Li_2CO_3 as the raw material had the best performance and maintained more than 90% of its initial capacity rate after 100 charge–discharge cycles at 1C rate. The as-synthesized $LiMn_2O_4$ delivered an initial discharge capacity of 109.1 and 104.2 mA h g^{-1} at 1C rate with the flower and flaky morphologies, respectively. Moreover, the as-synthesized spinel $LiMn_2O_4$ with micro-flower Li_2CO_3 exhibited an excellent cycling capability, maintaining 95% of its initial capacity after 200 cycles at a charge–discharge rate of 2C.

Experimental section

Li_2CO_3 synthesis

Battery grade Li_2CO_3 was synthesized through the reaction coupled with a solvent extraction process. First, LiCl (>97% pure, Beijing Yili, Fine, Chemical, Co., Beijing, China) was dissolved in deionized water. Then, 50 mL LiCl aqueous solution and 200 mL n-butanol (>97%, pure, Beijing, Chemical Works, Beijing, China), that served as the extracting agent and the diluent were added into a 500 mL separating funnel. The suspension was shaken for 15 min until the water phase and the alcohol phase reached equilibrium. Further, the upper alcohol phase was removed and added together with 100 mL tri-n-octyl amine (Alamine 336 – Sinopec, Beijing, China), which served as the extractant for HCl, to a three-necked flask. The reaction mixture was stirred at 150 rpm for approximately 45 min and then CO_2 (>95% pure, Tsinghua University, Beijing, China) was bubbled into the reactor at a pressure of 0.1 Mpa. The crystals obtained were then collected by filtration, washed with alcohol, and dried.

Synthesis of $LiMn_2O_4$

The as-synthesized Li_2CO_3 (0.50 g) along with 2.32 g MnO_2 were ground with high purity ethanol to produce a well-mixed powder. The powder was then calcinated by a two-step calcination at 650 °C and 800 °C for 5 hours with the heating rate at 3 °C min^{-1} in air to produce spinel $LiMn_2O_4$.

Characterization

The prepared Li_2CO_3 was mixed and reacted with MnO_2 (EMD, Xiangtan, Hunan) (molar ratio, $n(Li):n(Mn) = 1.01:2$). The nanostructured spinel $LiMn_2O_4$ was prepared by the solid-state combustion synthesis which is a two-step calcination process at 650 °C and 800 °C with the heating rate at 3 °C min^{-1} in air for 5 hours. The spinel $LiMn_2O_4$ formation process was studied by thermogravimetry (TG), derivative thermogravimetry (DTG) and differential scanning calorimetry (DSC). The crystal structure and morphology were identified by using X-ray diffraction analysis (XRD; D8-Advance, Bruker, Germany), scanning electron microscope (SEM; JSM7401, Jeol, Japan), and Tabletop scanning electron microscope (TM3000, Hitachi, Japan). Particle size distribution was measured by Malvern particle size analyzer (Mastersizer2000, Malvern, England). The Li concentration was analysed by using atomic absorption spectrophotometer (Z-5000-AAS, Hitachi, Tokyo, Japan). The purity of the as-synthesized Li_2CO_3 was determined by ICP-AES (Varian, 700-ES, USA).

Electrochemical measurement

Electrochemical measurements were performed by the coin cell which was prepared in an argon atmosphere inside a Glove Box (MIKROUNA, GER). The electrodes for electrochemical studies were prepared by making a slurry containing 85 wt% active material of $LiMn_2O_4$, 10 wt% conducting carbon black, and 5 wt% polyvinylidene fluoride (PVDF) binder in N-methyl-2-pyrrolidone (NMP) as a solvent. The slurry was applied onto an etched aluminum foil current collector using a doctor-blade and dried at 130 °C for 12 h in a vacuum oven. The coated cathode foil was then pressed to form a uniform layer and cut into a square sheet. Lithium metal foil was used as the anode. A 1 M solution of $LiPF_6$ in ethylene carbonate/dimethyl carbonate (EC/DMC, 1:1 v/v) was used as the electrolyte with a Cegrad 2400 membrane as a separator. The charge–discharge cycles were performed at different C rates between 3.0–4.3 V at room temperature using LAND battery testers.

Result and discussion

Synthesis, structure and morphology of Li_2CO_3

The synthesis of Li_2CO_3 is described in the Experimental section. The reaction process was coupled with the solvent extraction process, which is a new approach for producing Li_2CO_3 from LiCl and CO_2. The equation for the overall reaction as follows:

$$2LiCl + CO_2 + H_2O + 2S \rightarrow Li_2CO_3 + 2S \cdot HCl$$
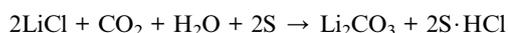
where S is referred to the extractant alamine 336. Three types of morphologies of Li_2CO_3 were synthesized by changing the initial concentration of LiCl. The flaky, flower-like, and nanorod

particles were prepared with the initial concentration of LiCl at 2, 3, 4, and 5 mol L^{-1} (Fig. 1a–d, respectively). The purity of the as-synthesized Li_2CO_3 was tested by ICP-MS with the mass fraction higher than 99.95% (see Table S1 in the ESI†). By comparing the purity of commercial Li_2CO_3, the as-synthesized Li_2CO_3 has purity higher than that of the required battery Li_2CO_3 (99.5%). With such high purity of raw material, the as-synthesized $LiMn_2O_4$ also exhibited a higher purity, which can improve the electrochemical performance of all sides of the surface of the resultant cathode. SEM images showed that the higher was the concentration of LiCl solution, the smaller was the particle size obtained. Thus, at a low concentration of LiCl, the synthesized crystals typically consisted of the flaky and the flower-like morphologies with micron size, while the nanorod particles were obtained with a high concentration of LiCl solution. Particle size distribution showed that the crystals were in micron and nanometer range with an approximate size of 8 ± 1 μm and 80 ± 10 nm (Fig. 1f), which are consistent with SEM images. The XRD patterns of the reaction-extraction of as-synthesized Li_2CO_3 correspond to JCPDS data no. 87-0729, and no additional impurity peaks were detected (Fig. 1e). Three different crystal morphologies are involved in two types of crystallization mechanism (see the explanation in the ESI†).

Synthesis, structure and morphology of $LiMn_2O_4$

Spinel $LiMn_2O_4$ was synthesized by a traditional solid-state calcination reaction by using the prepared Li_2CO_3 of three different morphologies as the raw materials. To optimize the structure, morphology and size of the as-synthesized spinel

$LiMn_2O_4$, the formation process was studied by thermogravimetry (TG), derivative thermogravimetry (DTG) and differential scanning calorimetry (DSC) (Fig. 2a). The weight loss of the mixtures occurred at two discrete regions of 30–650 °C and 700–800 °C and terminated at 800 °C. The weight loss at the temperature range of 30–650 °C is attributed to the loss of water followed by the decomposition of MnO_2, whose exothermic peak concentrated at 450–550 °C in the DTG curve. The weight loss at the temperature range of 700–800 °C and a large exothermic peak at 800 °C in the DTG curve can be considered as the result of the formation of spinel $LiMn_2O_4$. Two exothermic peaks were observed in the DSC curve at the temperature of 480 °C and 820 °C. The possible chemical reactions occurring in the synthesis of spinel $LiMn_2O_4$ was as follows:

$$4MnO_2 \rightarrow 2Mn_2O_3 + O_2$$

$$2Li_2CO_3 + 4Mn_2O_3 \rightarrow 4LiMn_2O_4 + CO_2$$
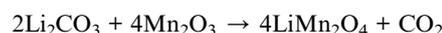
The calcination procedure was programmed following a two-step calcination at 650 °C and 800 °C for 5 hours with the heating rate at 3 °C min^{-1} in air.

Fig. 2b shows the XRD patterns of the products. All the samples were synthesized under the same reaction conditions. The $LiMn_2O_4$ XRD diffraction diagram shows the features of the spinel structure with Fd^3m space group (JCPDS card no. 35-0782), with no peaks of the Li_2CO_3 phase detected. The characteristic peaks of planes such as [111], [311], [222], [400], [331], [511], [440] and [531] can be clearly identified. Thus, the
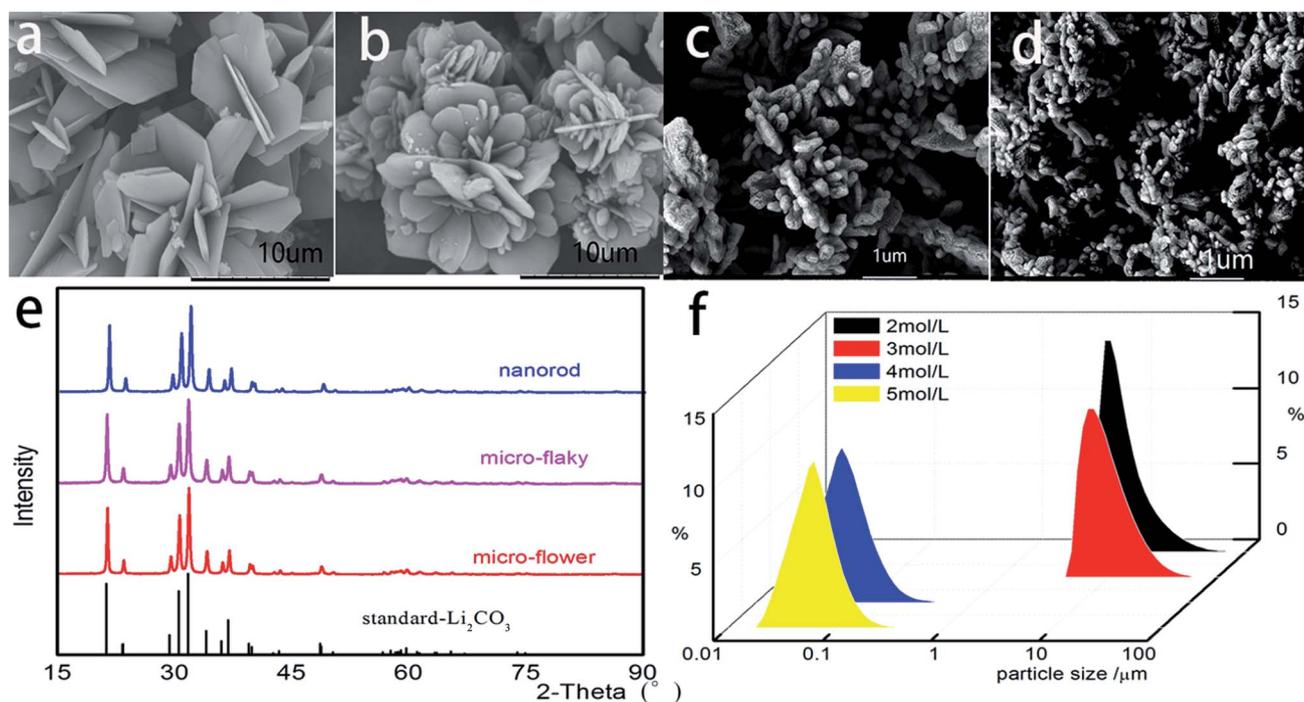

Fig. 1   SEM images, XRD pattern and particle-size distribution of the as-synthesized Li_2CO_3. (a) Micro-flaky, (b) micro-flower and (c, d) nanorod Li_2CO_3 with the initial concentration of LiCl at 2, 3, 4 and 5 mol L^{-1}, respectively, (e) XRD pattern, and (f) particle size distribution of the as-synthesized Li_2CO_3.
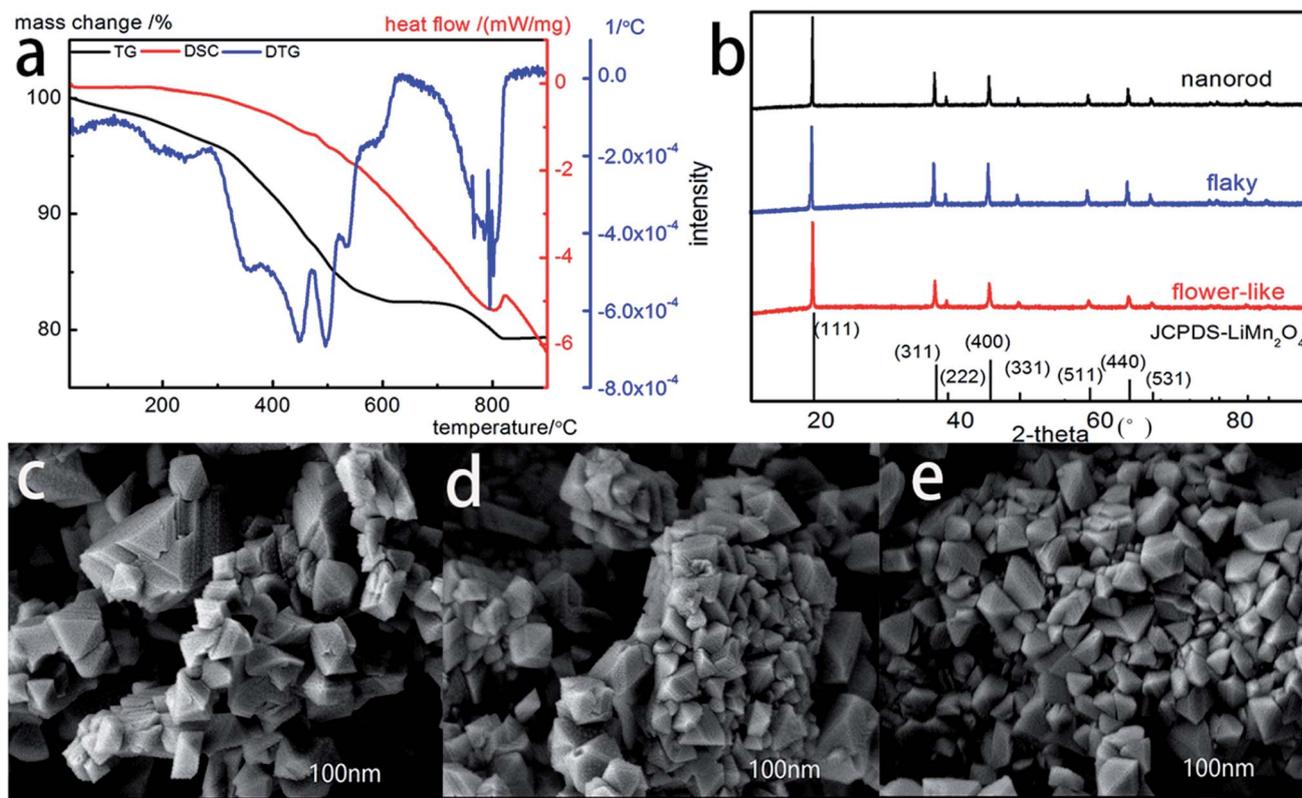
Fig. 2 (a) TG, DTG and DSC curves of the mixtures of Li_2CO_3 and MnO_2 with the ratio of $n(Li)/n(Mn) = 1.01 : 2$, (b) XRD patterns, and (c–e) SEM images of the as-synthesized spinel $LiMn_2O_4$ with the cathode material Li_2CO_3 in micro-flaky, micro-flower, and nanorod morphologies, respectively.

reaction between MnO_2 and Li_2CO_3 produced the pure $LiMn_2O_4$ phase. To analyze the morphological differences of $LiMn_2O_4$ prepared with different morphologies of Li_2CO_3, the SEM method was applied. Fig. 2c–e show that the synthesized products are highly crystalline and exhibit spinel structure along with the three types of Li_2CO_3 shown in Fig. 1a–c, respectively. It can be seen that the spinel structure displayed in Fig. 2c and d is more uniform than that shown in Fig. 2e. The distinctive, well-defined crystal faces exhibit the single spinel crystals of octahedral shape with well-developed planes. The as-synthesized spinel $LiMn_2O_4$ has an average size of 100 nm.

Electrochemical performance

The electrochemical measurements of three types of cathode materials were performed on the coin cell. The as-synthesized $LiMn_2O_4$ with flaky, flower-like and nanorod Li_2CO_3 forms is abbreviated as E1, E2, and E3, respectively. The galvanostatic charge/discharge tests were performed at room temperature and shown in Fig. 3a. The first charge and discharge curves were carried out at a current density of 1C. It delivered an initial charge capacity of 110.1, 105.2 and 104.9 mA h g^{-1} followed by a discharge capacity of 109.1, 103.9 and 104.2 mA h g^{-1} with Li_2CO_3 in micro-flower, nanorod and micro-flaky morphologies, respectively, at room temperature (about 99% of the charge capacity is discharged). The discharge specific capacity of the three types of cathode materials, which were prepared from the

same preparation route, as a function of cycle number has been compared with each other (Fig. 3b). The charge and discharge capacity was measured with the power rate at 1C (148 mA g^{-1}). It was observed that E1 and E2 had a much higher charge capacity than E3. Moreover, E1 and E2 showed better stability since their capacities were maintained at 94.2 mA h g^{-1} and 99.2 mA h g^{-1} after 100 cycles at the 1C rate, respectively. On the other hand, the discharge capacity decreased to 28.2 mA h g^{-1} in E3. The capacity retention was more than 90% at 100th cycle with the micron-sized Li_2CO_3.

To better understand the correlation between the structure and the electrochemical performance of the spinel $LiMn_2O_4$ prepared with the raw material of micron-sized Li_2CO_3, the TEM images and the ED patterns of $LiMn_2O_4$ E2 were analyzed. The results are shown in Fig. 4. TEM images and diffraction patterns showed that spinel $LiMn_2O_4$ is a cubic single crystal. To obtain excellent battery performance, the surface of the active materials is a very important factor. Based on the facet plane, one can conclude that the surface of this spinel $LiMn_2O_4$ is very pure and clean. The results showed that it is advantageous to obtain uniform cubic spinel nanostructured $LiMn_2O_4$ with micron-sized Li_2CO_3 as the raw material. The excellent cycle performance is possibly because the spinel $LiMn_2O_4$ prepared with the micron sized Li_2CO_3 and MnO_2 has a better particle size distribution and uniform morphology. Particle size distribution of the micron-sized Li_2CO_3 raw material was limited to a narrow
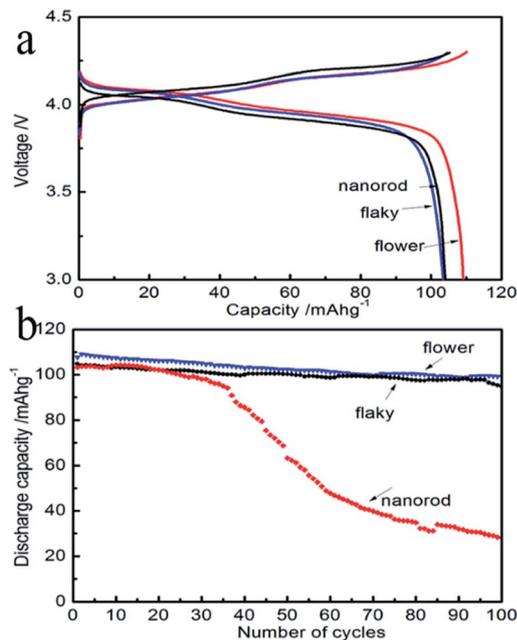
Fig. 3 (a) The charge and discharge curves at 1C rate of the as-synthesized spinel $LiMn_2O_4$ with the raw material Li_2CO_3 in micro-flower, micro-flaky and nanorod. (b) The discharge capacity of curves of the as-synthesized spinel $LiMn_2O_4$ with the cathode material Li_2CO_3 in micro-flower, micro-flaky and nanorod vs. number of cycles at 1C rate.
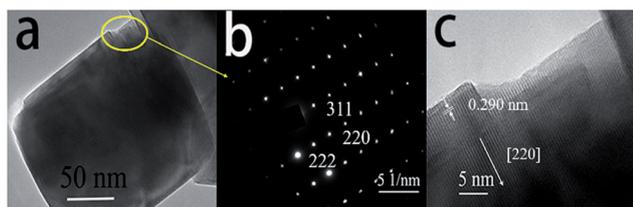

Fig. 4 (a and b) Low and high resolution TEM of $LiMn_2O_4$ with the cathode material Li_2CO_3 in micro-flower morphology, and (c) the electron diffraction pattern of $LiMn_2O_4$.

micron range; thus, it resulted in the uniform cubic spinel morphology of $LiMn_2O_4$. They were fused together forming a polyhedral structure which made the Li^+ entering the surface of the spinel diffuse through the huge inner structure. Moreover, the high purity of the as-synthesized Li_2CO_3 also plays a key positive role on the electrochemical performance of the as-synthesized $LiMn_2O_4$. The TEM images and the electron diffraction patterns also confirmed the cubic spinel structure of the as-synthesized $LiMn_2O_4$.

The specific surface area has a significant effect on the electrochemical performance of the as-synthesized spinel $LiMn_2O_4$. Thus, the specific surface areas of the as-synthesized Li_2CO_3 and $LiMn_2O_4$ were analyzed. The results showed that the specific surface area of nanosized Li_2CO_3 was larger than that of the micron-sized Li_2CO_3 (Fig. 5a), which indicates that the particle size of micron-sized Li_2CO_3 was larger than that of nano-sized Li_2CO_3. However, the as-synthesized spinel $LiMn_2O_4$
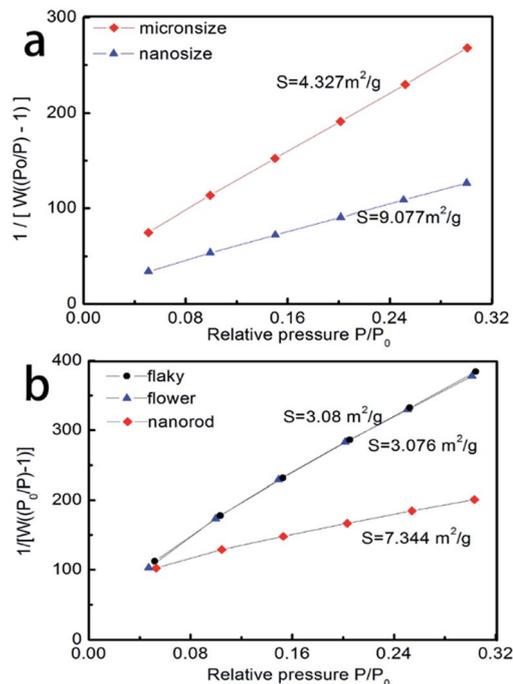

Fig. 5 (a) The specific surface area of the as-synthesized Li_2CO_3 and (b) the specific surface area of the as-synthesized $LiMn_2O_4$.

(Fig. 5b) with micron-sized Li_2CO_3 represented a smaller specific surface area. This exhibited an adverse result to the specific surface area of Li_2CO_3. The as-synthesized $LiMn_2O_4$ with micron-sized Li_2CO_3 showed a similar specific surface area (3.08 m^2 g^{-1} and 3.076 m^2 g^{-1}, respectively) while the as-synthesized $LiMn_2O_4$ with nano-sized Li_2CO_3 exhibited a higher specific surface area (7.344 m^2 g^{-1}). Moreover, the results showed that the excellent electrochemical performance was probably because of the smaller specific surface area of the as-synthesized $LiMn_2O_4$.

Fig. 6a shows the discharge capacity of $LiMn_2O_4$ E2 with the power rate at 2C. Its capacity was maintained at 87.5 mA h g^{-1} after 200 cycles at this rate. The capacity retention is about 95% at 200th cycle. The inset illustrates the charge–discharge curves of $Li/LiMn_2O_4$ cells. It can clearly be seen that the samples have two voltage plateaus at approximately 4.0 and 4.1 V, which is a typical feature of the spinel $LiMn_2O_4$. Two voltage plateaus specify that the insertion and extraction of lithium ion occurred in two stages. The first voltage plateau, at about 4.0 V, is attributed to the removal of lithium ions from half of the tetrahedral sites in which Li–Li interactions occur. The second voltage plateau observed at about 4.1 V is due to the removal of lithium ions from the other tetrahedral sites, in which lithium ions do not have Li–Li interactions. Fig. 6b illustrates the discharge specific capacity at various rates; the charge capacity was measured with the power rate from 0.2C (29.6 mA h) to 5C (740 mA h). It is observed that the as-synthesized spinel $LiMn_2O_4$ has a much higher discharge capacity than the commercial powders at different power rates. At the lowest value of current (from cycle 1 to 10), the sample has a specific capacity of 107.8 mA h g^{-1}. By increasing the rate to 1C, the
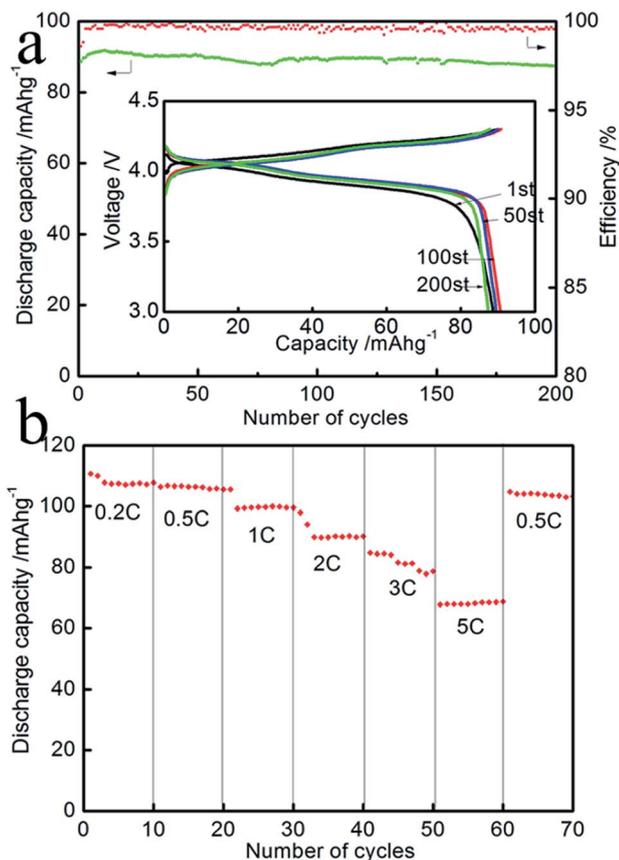
Fig. 6 (a) Discharge specific capacity and efficiency curves *vs.* number of cycles at the 2C rate. The inset image in (a) is the charge and discharge curves of LiMn$_2$O$_4$ at the 2C rate, and (b) the discharge capacity of spinel LiMn$_2$O$_4$ at various charge–discharge currents.

sample still has a discharge capacity of 100 mA h g^{-1}. The discharge capacity can return to 104 mA h g^{-1} at the 0.5C rate after the high rate discharge cycles, resulting in excellent cycle performance. The rate performance of E1 and E3 are shown in Fig. 7. The results show that E1 delivered a better rate performance. By analyzing the cycle performance and rate
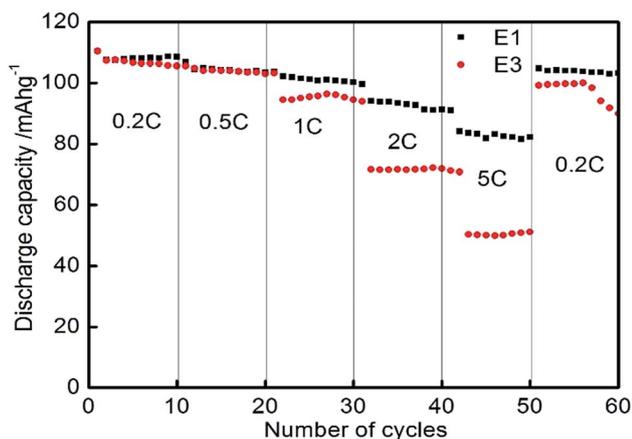

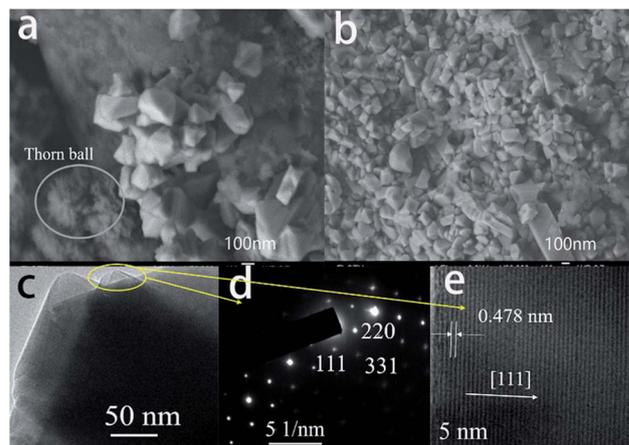**Fig. 7** Comparison of E1 and E3 at different charge–discharge currents.

Fig. 8 (a and b) SEM images of spinel LiMn$_2$O$_4$ after 200 cycles, the thorn ball besides the spinel LiMn$_2$O$_4$ was detected to be impurities. (c) Low and (d), high resolution TEM of spinel LiMn$_2$O$_4$ after 200 cycles at the 2C rate. And (e) the electron diffraction pattern image of spinel LiMn$_2$O$_4$ after 200 cycles at the 2C rate.

performance results of E1, E2 and E3, it is observed that the as-synthesized LiMn$_2$O$_4$ with micron-level Li$_2$CO$_3$ shows a better electrochemical performance. The better cycle and rate performance are owing to the smaller specific surface area of the as-synthesized LiMn$_2$O$_4$.

The anode lithium metal foil was immersed in the electrolyte for 6 hours, then washed with alcohol and dried in a vacuum dryer before the analysis methods were conducted. SEM images of spinel LiMn$_2$O$_4$ after 200 cycles are shown in Fig. 8a and b. It is seen that the spinel structure was maintained after 200 cycles. The impurity was detected at the same time as shown in Fig. 8a as a thorn ball was located besides the spinel LiMn$_2$O$_4$. It is probably because LiMn$_2$O$_4$ had not been washed throughout, while as shown in Fig. 8b the pure spinel LiMn$_2$O$_4$ was detected without any impurity phases existing. Moreover, TEM was tested to determine the cubic spinel structure of LiMn$_2$O$_4$. From the images shown in Fig. 8c–e, clear lattice images were observed. The electron diffraction patterns indicate that the single crystalline cubic spinel structure is maintained after 200 cycles. The plane [111] is observed in the TEM images with a lattice parameter of 0.478 nm which corresponds to one of the peaks of LiMn$_2$O$_4$.

Conclusion

The cubic spinel LiMn$_2$O$_4$ was synthesized with three different morphologies of the raw material Li$_2$CO$_3$ by the solid-state calcination synthesis. The effects of Li$_2$CO$_3$ with micro-flaky, micro-flower and nanorod morphologies on the electrochemical properties of spinel LiMn$_2$O$_4$ were analyzed. The electrochemical measurements showed that the as-synthesized spinel LiMn$_2$O$_4$ (E1, E2 and E3) delivered a discharge capacity of 104.2, 109.1 and 103.9 mA h g^{-1} at the 1C charge–discharge rate. The results showed that the as-synthesized spinel LiMn$_2$O$_4$ with micron sized Li$_2$CO$_3$ exhibited excellent electrochemical

cyclability because of its well-crystalline nanostructure, and it maintained more than 90% of its initial capacity after 100 charge–discharge cycles at the 1C rate. Moreover, the as-synthesized spinel $LiMn_2O_4$ E2 retained more than 95% of its initial discharge capacity after 200 cycles at the 2C rate. The cubic spinel structure was detected after 200 cycles of $LiMn_2O_4$ at this rate. By comparing three types of morphologies of raw material Li_2CO_3, the Li_2CO_3 particles with micron size were found to be more suitable than those of nano size for calcination with MnO_2 to produce the cubic spinel $LiMn_2O_4$.

Conflicts of interest

There are no conflicts to declare.

Abbreviation

E1	$LiMn_2O_4$ with micro-flaky as raw material
E2	$LiMn_2O_4$ with flower as raw material
E3	$LiMn_2O_4$ with nanorod Li_2CO_3 as raw material

Acknowledgements

References

1 J. Y. Luo and Y. Y. Xia, *Adv. Funct. Mater.*, 2010, **17**, 3877–3884.

2 X. Liu, G. Zhu, K. Yang and J. Wang, *J. Power Sources*, 2007, **174**, 1126–1130.

3 P. G. Bruce, S. A. Freunberger, L. J. Hardwick and J. Tarascon, *Nat. Mater.*, 2012, **11**, 19–29.

4 J. Li, M. Wei, W. Chu and N. Wang, *Chem. Eng. J.*, 2017, **316**, 277–287.

5 A. S. Wills, N. P. Raju and J. E. Greedan, *Chem. Mater.*, 1999, **11**, 1510–1518.

6 Q. C. Zhuang, T. Wei, L. L. Du, Y. L. Cui and L. Fang, *J. Phys. Chem. C*, 2010, **114**, 8614–8621.

7 H. L. Zhu, Z. Y. Chen, S. Ji and V. Linkov, *Solid State Ionics*, 2008, **179**, 1788–1793.

8 R. Singhal, S. R. Das, O. Oviedo, M. S. Tomar and R. S. Katiyar, *J. Power Sources*, 2006, **160**, 651–656.

9 C. H. Lu, Y. Lin and H. C. Wang, *J. Mater. Sci. Lett.*, 2003, **22**, 615–618.

10 S. Nieto, S. B. Majumder and R. S. Katiyar, *J. Power Sources*, 2004, **136**, 88–98.

11 H. Uchiyama, E. Hosono, H. Zhou and H. Imai, *J. Mater. Chem.*, 2009, **19**, 4012–4016.

12 K. M. Shaju and P. G. Bruce, *Chem. Mater.*, 2008, **20**, 5557–5562.

13 Q. Qu, L. Fu, X. Zhan, D. Samuelis, J. Maier, L. Li, S. Tian, Z. Li and Y. Wu, *Energy Environ. Sci.*, 2011, **4**, 3985–3990.

14 D. K. Kim, P. Muralidharan, H. Lee, R. Ruffo, Y. Yang, C. K. Chan, H. Peng, R. A. Huggins and Y. Cui, *Nano Lett.*, 2008, **8**, 3948–3952.

15 W. Tang, Y. Hou, F. Wang, L. Liu and Y. Wu, *Nano Lett.*, 2013, **13**, 2036–2040.

16 H. Xia, K. R. Ragavendran, J. Xie and L. Lu, *J. Power Sources*, 2012, **212**, 28–34.

17 Y. Ding, J. Xie, G. Cao, T. Zhu, H. Yu and X. Zhao, *Adv. Funct. Mater.*, 2011, **21**, 348–355.

18 E. Hosono, T. Kudo, I. Honma, H. Matsuda and H. Zhou, *Nano Lett.*, 2009, **9**, 1045–1051.

19 H. W. Lee, P. Muralidharan, R. Ruffo, C. M. Mari and Y. Cui, *Nano Lett.*, 2010, **10**, 3852–3856.

20 S. Lee, Y. Cho, H. K. Song, K. T. Lee and J. Cho, *Angew. Chem., Int. Ed.*, 2012, **51**, 8748–8752.

21 J. Luo, X. Li and Y. Xia, *Electrochim. Acta*, 2007, **52**, 4525–4531.

22 X. He, L. Wang, W. Pu and G. Zhang, *Int. J. Electrochem. Sci.*, 2006, **1**, 12–16.

23 Y. K. Sun, I. H. Oh and K. Y. Kim, *Ind. Eng. Chem. Res.*, 1997, **36**, 4839–4846.

24 H. M. Wu, J. P. Tu, Y. F. Yuan, X. T. Chen and J. Y. Xiang, *J. Power Sources*, 2006, **161**, 1260–1263.

25 Y. Bi, T. Wang, M. Liu, R. Du and W. Yang, *RSC Adv.*, 2016, **6**, 19233–19237.

26 Z. Zhou, F. Liang, W. Qin and W. Fei, *AIChE J.*, 2014, **60**, 282–288.